

## Effects of Mountains and Ice Sheets on Global Ocean Circulation\*

ANDREAS SCHMITTNER AND TIAGO A. M. SILVA<sup>†</sup>

*Oregon State University, Corvallis, Oregon*

KLAUS FRAEDRICH, EDILBERT KIRK, AND FRANK LUNKEIT

*Universität Hamburg, Hamburg, Germany*

(Manuscript received 6 August 2010, in final form 24 November 2010)

### ABSTRACT

The impact of mountains and ice sheets on the large-scale circulation of the world's oceans is investigated in a series of simulations with a new coupled ocean–atmosphere model [Oregon State University–University of Victoria model (OSUVic)], in which the height of orography is scaled from 1.5 times the actual height (at T42 resolution) to 0 (no mountains). The results suggest that the effects of mountains and ice sheets on the buoyancy and momentum transfer from the atmosphere to the surface ocean determine the present pattern of deep ocean circulation. Higher mountains reduce water vapor transport from the Pacific and Indian Oceans into the Atlantic Ocean and contribute to increased (decreased) salinities and enhanced (reduced) deep-water formation and meridional overturning circulation in the Atlantic (Pacific). Orographic effects also lead to the observed interhemispheric asymmetry of midlatitude zonal wind stress. The presence of the Antarctic ice sheet cools winter air temperatures by more than 20°C directly above the ice sheet and sets up a polar meridional overturning cell in the atmosphere. The resulting increased meridional temperature gradient strengthens midlatitude westerlies by ~25% and shifts them poleward by ~10°. This leads to enhanced and poleward-shifted upwelling of deep waters in the Southern Ocean, a stronger Antarctic Circumpolar Current, increased poleward atmospheric moisture transport, and more advection of high-salinity Indian Ocean water into the South Atlantic. Thus, it is the current configuration of mountains and ice sheets on earth that determines the difference in deep-water formation between the Atlantic and the Pacific.

### 1. Introduction

The large-scale ocean circulation is an important component of the climate system, transporting heat, plant nutrients, carbon, oxygen, and other substances around the globe and connecting the atmosphere with the large reservoir of the deep sea. The processes that drive this circulation are not well understood in detail, although some general principles have been established. The importance of winds, for instance, is known to strongly affect

the surface circulation because of momentum transfer. However, winds also affect the deep ocean circulation, particularly in the Southern Ocean, where the strong meridional gradient in westerlies, which coincides with the location of Drake Passage, leads to the upwelling of deep water and enhanced production and export of North Atlantic Deep Water (NADW) in model simulations (Delworth and Zeng 2008; McDermott 1996; Rahmstorf and England 1997; Toggweiler and Samuels 1995).

Buoyancy forcing is also important in driving the global meridional overturning circulation. The Atlantic as a whole loses freshwater at the surface (Broecker et al. 1985). Resulting higher salinities of surface waters in the Atlantic compared to the Pacific lead to a fundamentally different circulation pattern in the two basins. Whereas salty and dense NADW sinks to 2–3-km depths, travels south as a deep western boundary current, and sets up a global meridional overturning circulation system, no such sinking is observed in the North Pacific, where fresh light surface waters float on top of salty subsurface waters

\* Supplemental information related to this paper is available at the Journals Online Web site: <http://dx.doi.org/10.1175/2010JCLI3982.s1>.

<sup>†</sup> Current affiliation: School of Environmental Sciences, University of East Anglia, Norwich, United Kingdom.

Corresponding author address: Andreas Schmittner, College of Oceanic and Atmospheric Sciences, Oregon State University, 104 COAS Admin. Bldg., Corvallis, OR 97331-5503.  
E-mail: [aschmitt@coas.oregonstate.edu](mailto:aschmitt@coas.oregonstate.edu)

(Weaver et al. 1999). Water vapor fluxes from the Pacific to the Atlantic by midlatitude westerly winds are blocked by the Rocky Mountains in North America and the Andes in South America, whereas the easterly trade winds in the tropics transport water vapor through gaps in the mountain chains of Central America from the Atlantic to the Pacific. Although the configuration of mountains has long been implicated to contribute to the observed salinity contrast between the Atlantic and the Pacific (Dietrich and Kalle 1957; Weyl 1968), this effect and its implication on ocean circulation has not been quantified with a coupled ocean–atmosphere model.

Modeling the global ocean circulation remains a challenge. Early coarse-resolution coupled ocean–atmosphere models required flux corrections—that is, artificial heat, water, or momentum fluxes at the air–sea interface—to simulate a realistic overturning circulation (Manabe and Stouffer 1994), perhaps related to the too-coarse representation of mountains (Lohmann 2003; Zaucker and Broecker 1992). Although some modern, higher-resolution models simulate realistic deep-water formation rates and temperature and salinity distributions in good agreement with hydrographic observations, other models—for example, some of those that contributed to the Intergovernmental Panel on Climate Change Fourth Assessment Report (IPCC AR4)—have large errors in both hydrographic fields and mass fluxes (Schmittner et al. 2005).

Here we attempt to further our understanding of the processes that drive the ocean circulation in coupled ocean–atmosphere models by studying the orographic effects of mountains and ice sheets. Model studies of the effects of mountains on the atmospheric circulation and climate have a long tradition (Kitoh 2002; Manabe and Terpstra 1974); however, to our knowledge, no study to date has investigated the effects on the global ocean circulation. We will show that mountains and ice sheets influence both buoyancy and momentum fluxes to the surface ocean that conspire to generate strong deep-water formation in the North Atlantic and set up the known pattern of the global ocean overturning circulation.

## 2. Model description

We use a new ocean–atmosphere model [Oregon State University–University of Victoria model (OSUVic), version 0.3] that combines ocean, sea ice, land surface, and ocean biogeochemical model components from the UVic Earth System Model, version 2.8 (Weaver et al. 2001), with the simplified atmospheric general circulation model Planet Simulator, version 15.043 (Fraedrich et al. 2005a,b). The complete Planet Simulator model, including sources and documentation, is available online ([www.mi.uni-hamburg.de/](http://www.mi.uni-hamburg.de/)

plasm). The Planet Simulator solves the primitive equations and includes the hydrological cycle, clouds, and a simple radiation scheme. We use Planet Simulator at two horizontal resolutions: T21  $\sim(5.6^\circ \times 5.6^\circ)$  and T42  $\sim(2.8^\circ \times 2.8^\circ)$ , with 10 vertical sigma levels and without a gravity-wave drag parameterization (Boer and Lazare 1988). The UVic model is used at the same resolution ( $1.8^\circ \times 3.6^\circ$ , 19 levels) and configuration with a closed Bering Strait in all the numerical experiments described in this paper as described in more detail in Schmittner et al. (2008). The models are coupled through fluxes of momentum, heat, and water at the air–sea interface using the Ocean Atmosphere Sea Ice Soil, version 3 (OASIS3), coupler ([www.prism.enes.org/PAEs/coupling\\_IO/software\\_OASIS3.php](http://www.prism.enes.org/PAEs/coupling_IO/software_OASIS3.php)) to map between the different grids. No flux adjustments are used. More detailed information about OSUVic, the coupling, and comparison with observations can be found in the supplementary material (<http://dx.doi.org/10.1175/2010JCLI3982.s1>) and at the author's Internet site (<http://mkg.coas.oregonstate.edu/~andreas/OSUVic>).

## 3. Experimental setup

To investigate the impact of mountains and ice sheets on climate and ocean circulation, we have conducted four experiments that differ only in the height of orography over land. This was achieved by multiplying the default orography in the T42 model version with a constant scaling factor (OROSCALE).  $\text{OROSCALE} = 1$  corresponds to a realistic orography at T42 resolution (Fig. 1);  $\text{OROSCALE} = 0$  corresponds to a flat world; and  $\text{OROSCALE} = 0.5$  and  $\text{OROSCALE} = 1.5$  simulate a world with 50% lower and higher mountains, respectively. All other model parameters and forcings are identical. Note that this setup does not consider changes in river routing and vegetation type that would accompany orographic variations and their influences on albedo, roughness length, and water fluxes. The model at T21 resolution has a few parameters adjusted to simulate a realistic mean climate comparable to the T42 version.

The models were started from identical initial conditions taken from the *World Ocean Atlas* (Antonov et al. 2006; Locarni et al. 2006) and integrated for 500–600 yr. The atmosphere, surface, and upper ocean are close to equilibrium at the end of the integrations; however, the deep ocean is not.

## 4. Results

During the first 25 yr, all models simulate a very similar evolution of the Atlantic meridional overturning circulation (AMOC) starting at around 18 Sv ( $1 \text{ Sv} \equiv 10^6 \text{ m}^3 \text{ s}^{-1}$ ) at year zero and decreasing to 12–14 Sv around year 25 (Fig. 2). After year 25, however, the simulations diverge,

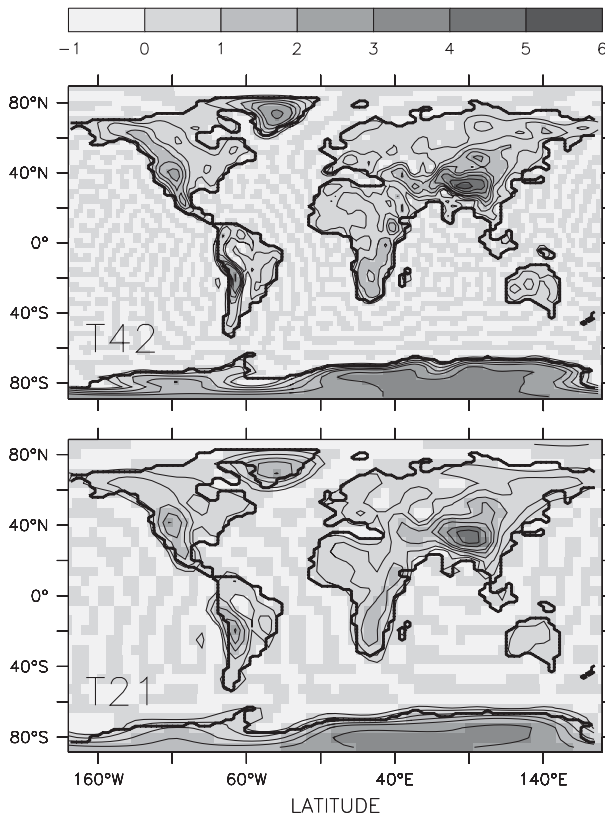


FIG. 1. Orography (km) at (bottom) T21 and (top) T42 resolution from the atmospheric model component (Planet Simulator). Isolines are shown at 200 and 500 m, and at 1, 1.5, 2, 3, 4, 5, and 6 km. Here the orography is the surface geopotential divided by Earth's gravitational acceleration  $g = 9.8 \text{ m s}^{-2}$ . The speckled pattern over the oceans is due to the Gibbs effect. The thick contour line shows the land–sea distribution (coastlines) from the ocean–land surface model components (UVic).

such that models with higher mountains lead to a stronger circulation. All models show small interannual to decadal fluctuations of  $\sim 2$  Sv. The models with realistic or higher mountains (OROSCALE = 1 and OROSCALE = 1.5, respectively) and the model at T21 resolution experience the long-term trend of the AMOC after year 150 and appear statistically to be close steady state. Conversely, the models with lower mountains continue to drift toward a weaker AMOC even after year 200, indicating that they are not in equilibrium. At the end of the flat-world simulation, no deep water is forming in the North Atlantic. The average salinity in the Atlantic north of  $35^\circ\text{S}$  decreases linearly throughout the flat-world integration from 35.01 to 34.83, and surface waters of the North Pacific becomes saltier than those in the North Atlantic (not shown), triggering deep-water formation there. This suggests that the state without deep-water formation in the North Atlantic is stable although no reverse circulation cell is apparent in the South Atlantic, the existence of

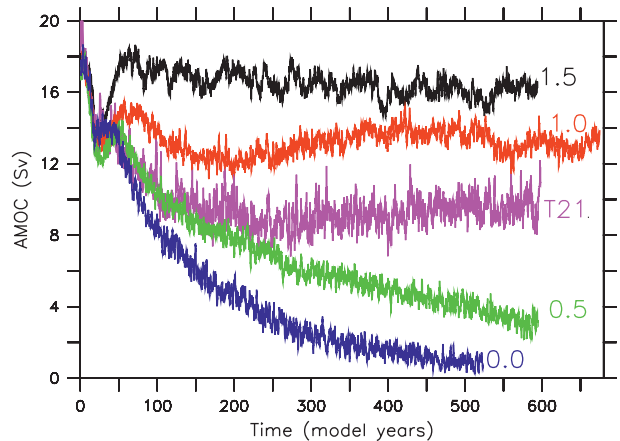


FIG. 2. Twelve-month running-mean AMOC (Sv) at  $25^\circ\text{N}$  for different orographic scalings at T42 resolution of the atmospheric model (black: OROSCALE = 1.5; red: OROSCALE = 1; green: OROSCALE = 0.5; blue: OROSCALE = 0) and at T21 resolution (purple).

which has been suggested to be responsible for the stability of the “off” state in models with realistic topography (Gregory et al. 2003; Saenko et al. 2003a).

A weaker AMOC in the experiments with lower mountains and ice sheets (OROSCALE = 0 and OROSCALE = 0.5, respectively) is obvious in the patterns of the meridional overturning circulation (Fig. 3). Models with shallow or no orography develop a meridional overturning circulation cell in the North Pacific, in contrast to observations. Shallower mountains and ice sheets lead to a weaker and shallower Deacon cell (clockwise circulation between about  $60^\circ$  and  $40^\circ\text{S}$  from about 2–3-km depth to the surface in Fig. 3). The strength of the Deacon cell, measured as the maximum total (including eddy induced transport; not shown) streamfunction south of  $35^\circ\text{S}$  and below 300-m depth, decreases from 31 Sv in OROSCALE = 1.5 to 21 Sv in OROSCALE = 0.

Antarctic Bottom Water (AABW) formation increases and the associated polar meridional overturning cell between  $80^\circ$  and  $60^\circ\text{S}$  broadens and strengthens from  $\sim 6$  to  $\sim 12$  Sv as orography is lowered. The global bottom water meridional overturning cell (the counter clockwise cell below 1.5–2.5-km depth in Fig. 3) is very similar (10–12 Sv) in all simulations and does not seem to be affected by the increase in the polar AABW cell. Latitudes of important features of the meridional overturning circulation in the Southern Ocean—such as the upwelling of deep water, the maximum of the Deacon cell, as well as the zero streamfunction isoline that separates the Deacon cell from the polar AABW cell—are all shifted equatorward by up to  $10^\circ$  because of the lowering of orography.

The Antarctic Circumpolar Current (ACC) is faster the taller is the model orography (Fig. 4). Averaged flow

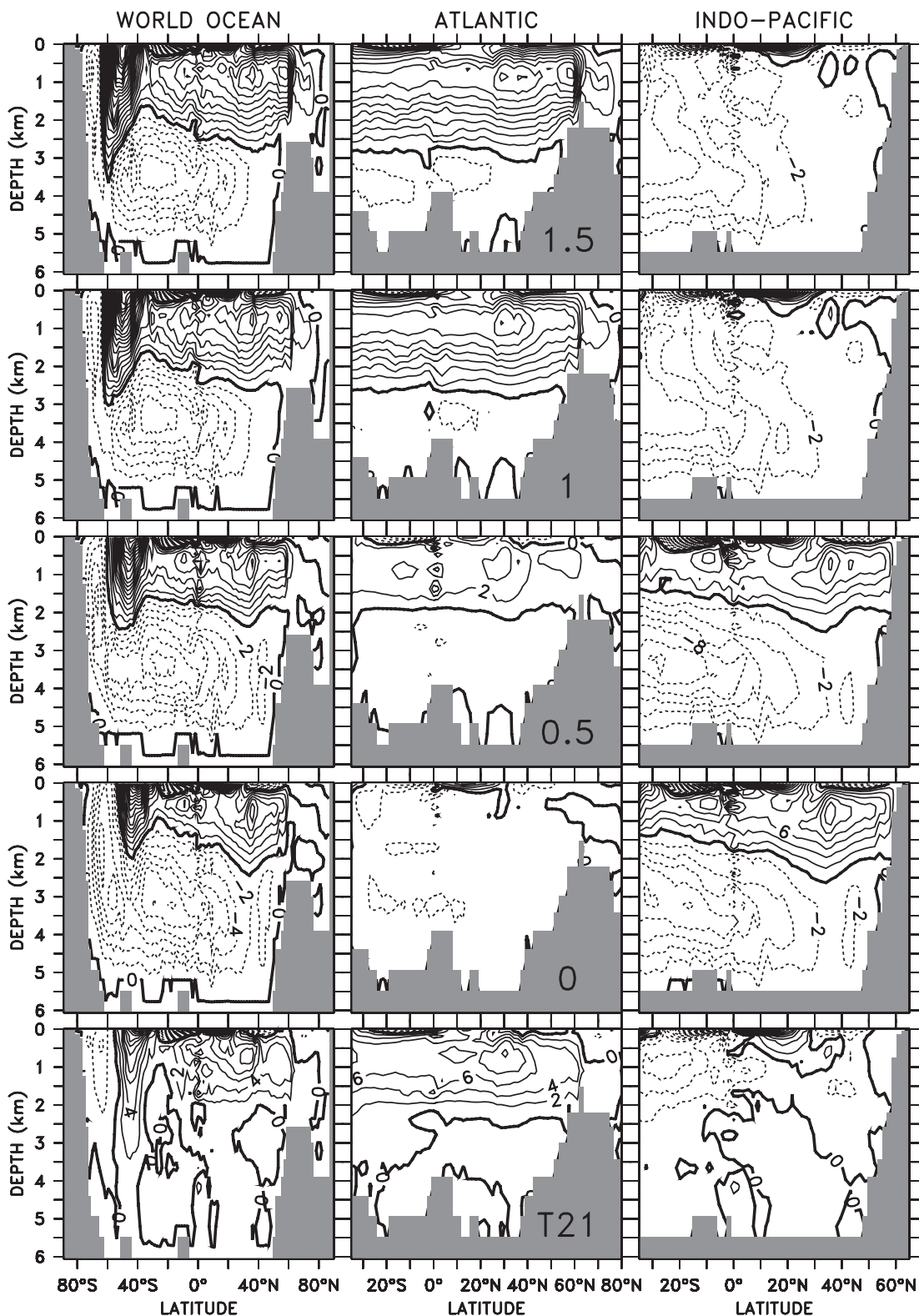


FIG. 3. Eulerian meridional overturning streamfunction (Sv) averaged between years 490–510 for the models with different orographic scaling at T42 resolution: OROSCALE (top to next to bottom) = 1.5, 1, 0.5, and 0; and from the (bottom) T21-resolution model. Flow is clockwise along positive streamlines (solid) and counterclockwise along negative (dashed) streamlines.

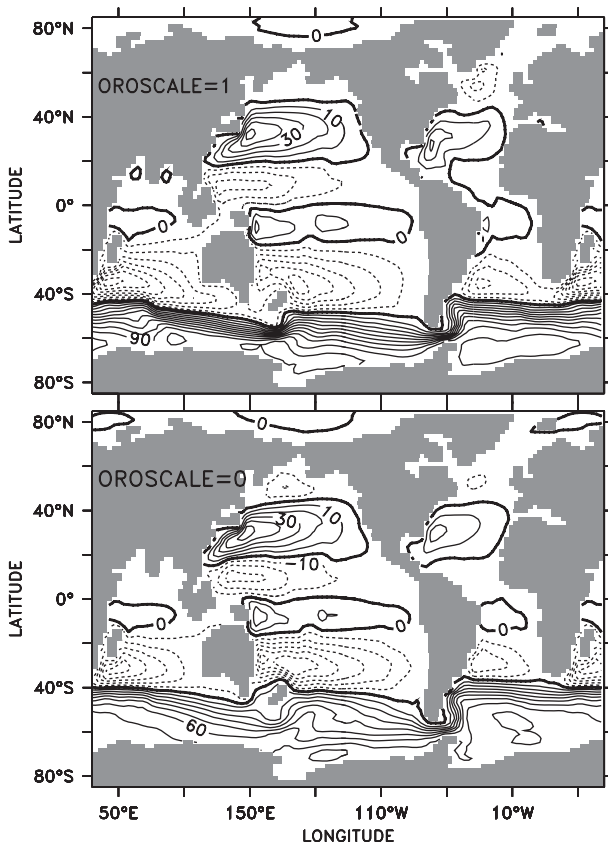


FIG. 4. Vertically integrated flow (Sv) for model with (top) regular orography and (bottom) the flat-world model. Positive (negative) values of the barotropic streamfunction indicate clockwise (counterclockwise) flow.

through Drake Passage during model years 450–470 is 105 Sv (OROSCALE = 1.5), 100 Sv (OROSCALE = 1), 85 Sv (OROSCALE = 0.5), and 72 Sv (OROSCALE = 0). For comparison, observational estimates of the ACC are around 130 Sv (Lumpkin and Speer 2007). The presence of mountains and ice sheets also lead to a much stronger flow of Indian Ocean water around the tip of South Africa into the Atlantic (15 Sv in OROSCALE = 1 vs 3 Sv in OROSCALE = 0). Flow through the Indonesian archipelago is doubled because of the presence of orography (18 Sv in OROSCALE = 1 vs 9 Sv in OROSCALE = 0).

The ocean circulation in the model at T21 resolution is inconsistent with observations because it shows a too weak AMOC, very little AABW formation, too weak and too shallow inflow of circumpolar deep water into the Indian and Pacific Oceans, too little and too far northward-shifted upwelling in the Southern Ocean, and a very weak (30 Sv) ACC. Reasons for the poor performance of the coarse (T21) atmospheric resolution model are discussed in the appendix.

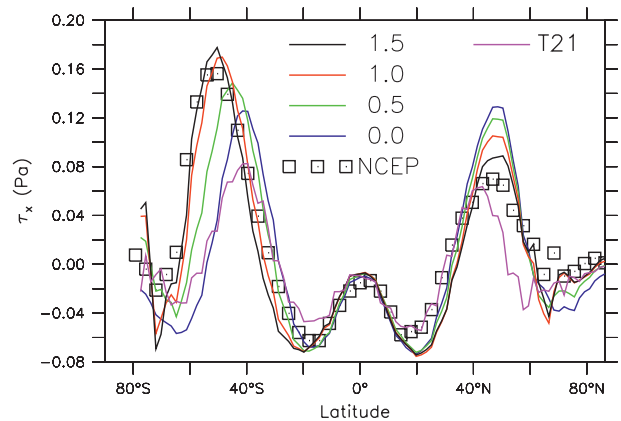


FIG. 5. Zonal-mean zonal wind stress (Pa) averaged between years 490 and 510 for models at T42 resolution with different topographical scaling (black: OROSCALE = 1.5; red: OROSCALE = 1; green: OROSCALE = 0.5; blue: OROSCALE = 0) and for the standard T21-resolution version (purple). Square symbols show the NCEP reanalysis data (Kalnay et al. 1996). Positive (negative) values denote westerly (easterly) winds.

## 5. Analysis

### a. Zonal wind stress

The large differences in circulation, particularly in the Southern Ocean, between the experiments with different orography discussed in the previous section, can be explained, at least partly, by changes in zonal wind stress. Mountains and ice sheets strongly affect the strength and pattern of zonal-mean wind stress at the sea surface

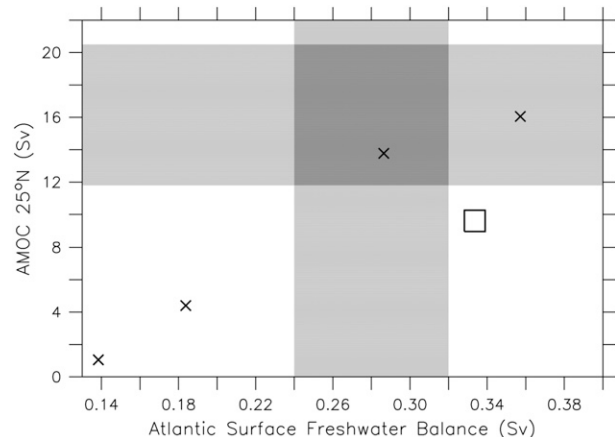


FIG. 6. The AMOC at 25°N vs Atlantic surface freshwater budget. Symbols are averages from model years 490–510 for the four model versions with different orographic scaling at T42 resolution (× symbols) and the model at T21 resolution (square). Shading represents observational estimates of the freshwater budget ( $0.28 \pm 0.4$  Sv) by Talley (2008) and the AMOC at 24°N ( $14.1 \pm 2.3$  Sv) by Wunsch and Heimbach (2006) and ( $18.0 \pm 2.5$  Sv) by Lumpkin and Speer (2007).

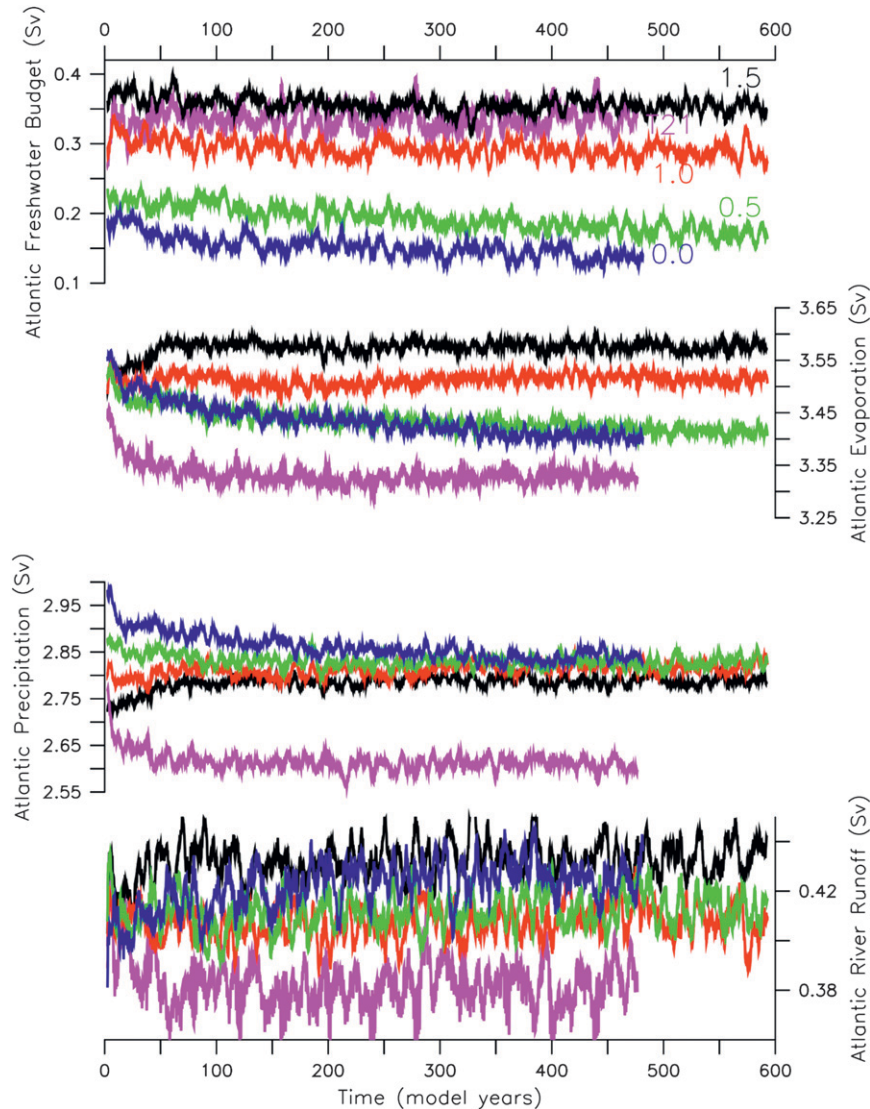


FIG. 7. Evolution of Atlantic surface freshwater budget integrated north of  $35^{\circ}\text{S}$  and its individual terms— $E$ ,  $P$ , and  $R$ —for the models with different topographic scaling at T42 resolution (black, red, green, and blue) and the model at T21 resolution (purple).

outside of the tropics (Fig. 5). Models with lower orography display weaker westerlies in the Southern Hemisphere and stronger westerlies in the Northern Hemisphere. Weaker westerlies in the Southern Hemisphere are consistent with, and presumably an important reason for, the slower ACC in the models with shallower orography, although changes in buoyancy fluxes may also influence the ACC (Marshall and Radko 2003). The latitude of maximum wind stress in the Southern Hemisphere is shifted equatorward by up to  $10^{\circ}$  by lower orography, explaining the corresponding latitudinal shift in upwelling and meridional circulation in the Southern Ocean discussed above (Fig. 3, section 4).

In the Northern Hemisphere, the latitude of maximum wind stress is not affected by orography. A large asymmetry between the hemispheres with more than 2 times stronger wind stress in the Southern Hemisphere than in the Northern Hemisphere is apparent in the observations as approximated by the National Centers for Environmental Prediction (NCEP) reanalysis data. The model with realistic mountains reproduces the observed asymmetry qualitatively (although it underestimates the interhemispheric differences because of overestimated wind stress in the Northern Hemisphere), whereas the model with flat orography displays an almost symmetrical distribution. This suggests that the observed asymmetry of

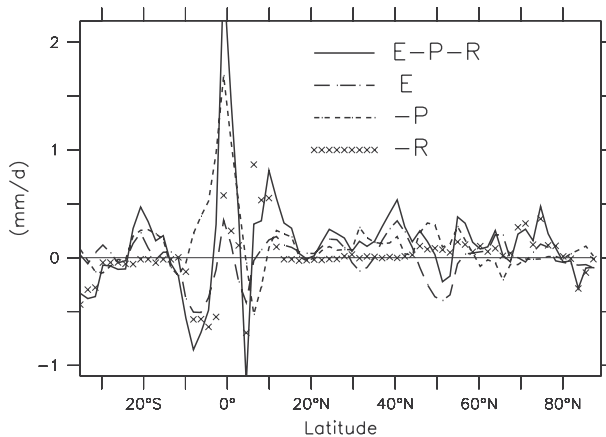


FIG. 8. Zonal-mean difference in Atlantic surface freshwater budget due to the presence of mountains (OROSCALE = 1 minus OROSCALE = 0) averaged for model years 20–22. Terms  $E$  (long dash), negative precipitation ( $-P$ ; short dash), and negative river runoff ( $-R$ ; symbol  $x$ ) are shown individually.

zonal wind stress between the hemispheres is a result of the presence of mountains and ice sheets on Earth.

Models with realistic or higher mountains and ice sheets generally show better agreement with observations than models with low or flat orography. However, westerly wind stress in the Northern Hemisphere, particularly over the North Pacific (not shown), is overestimated by the model with realistic orography, perhaps because of the neglecting of gravity-wave drag (Boer and Lazare 1988). This bias could lead to an overestimation of the shallow, wind-driven circulation in the North Pacific.

### b. Surface freshwater budgets

To understand why the AMOC differs so much between the different simulations, it is instructive to analyze the Atlantic surface freshwater budget. In the following analysis, we distinguish between evaporation  $E$ , precipitation  $P$ , and river runoff  $R$  in determining the total freshwater budget  $F = E - P - R$  of the Atlantic north of  $35^\circ\text{N}$ , which is, per definition, positive if the ocean loses water to the atmosphere. The effects of melting and freezing of sea ice on the surface freshwater budget are negligible on a basinwide scale and the long time scales considered here. The Atlantic is a net evaporative ( $F > 0$ ) ocean basin (Broecker et al. 1985). Close to equilibrium, the AMOC in the model at T42 resolution is approximately linearly related to the magnitude of this freshwater loss (Fig. 6), qualitatively consistent with earlier, more simplified models (Rahmstorf 1996; Stocker and Wright 1991). Comparison to recent observational estimates shows that in the models with shallow mountains (OROSCALE = 0.5 and OROSCALE = 0), the Atlantic is not losing enough freshwater at the surface and that the

AMOC is too weak. In the model with tall mountains (OROSCALE = 1.5), the Atlantic is evaporating too much; however, the AMOC is consistent with observations. The model with full mountains and ice sheets (OROSCALE = 1) has a realistic Atlantic surface freshwater budget, but the circulation is in the lower range of the observational estimates. Note that processes other than the basinwide surface freshwater budget influence the circulation, such as redistributions of freshwater within the Atlantic drainage basin (Gregory et al. 2003), ocean mixing, and wind stress. This is perhaps most obvious for the model at T21 resolution, which has a very weak AMOC despite a larger-than-observed evaporative freshwater budget.

Interestingly, the total surface freshwater budget of the Atlantic is set almost immediately after the start of the simulations because of fast atmospheric dynamics, and it changes little with time (Fig. 7, top panel). It ranges from  $\sim 0.37$  Sv for OROSCALE = 1.5 to  $\sim 0.16$  Sv for OROSCALE = 0. These results demonstrate the importance of mountains in controlling the magnitude of the Atlantic surface freshwater balance.

Individual terms in the freshwater budget vary much more in time than the total budget (Fig. 7, bottom panels). River runoff is very similar for all the simulations without obvious systematic differences between them. During the first years, evaporation is also very similar for all the runs, presumably because it is strongly influenced by sea surface temperatures (SSTs), which are still close to the initial conditions. In the simulations with shallow orography, North Atlantic SSTs slowly cool because of reduced ocean heat transport, which leads to decreasing evaporation, whereas in the high mountains experiment, SSTs and evaporation increase. Once the AMOC differences have been established after about 100 years, evaporation acts as a positive feedback (Warren 1983) and dominates the difference in the surface freshwater budget.

However, differences in precipitation are crucial in setting up the initial differences in the surface freshwater budget and therefore in controlling the early transitions to the different AMOC states. Initial differences in precipitation are greater than 0.2 Sv, accounting entirely for the differences in the initial surface freshwater budget. Although those large initial differences slowly decrease with time, the difference between the case without mountains and the one with high mountains (OROSCALE = 1.5) is still  $\sim 0.05$  Sv between years 450–470.

The Pacific north of  $35^\circ\text{S}$  receives more river runoff (0.55 Sv for OROSCALE = 1.5; 0.45 Sv for OROSCALE = 1; 0.3 Sv for OROSCALE = 0.5; and 0.23 Sv for OROSCALE = 0) and less precipitation (by  $\sim 0.1$ – $0.2$  Sv) the higher the mountains (not shown), whereas evaporation is similar between all experiments. These differences

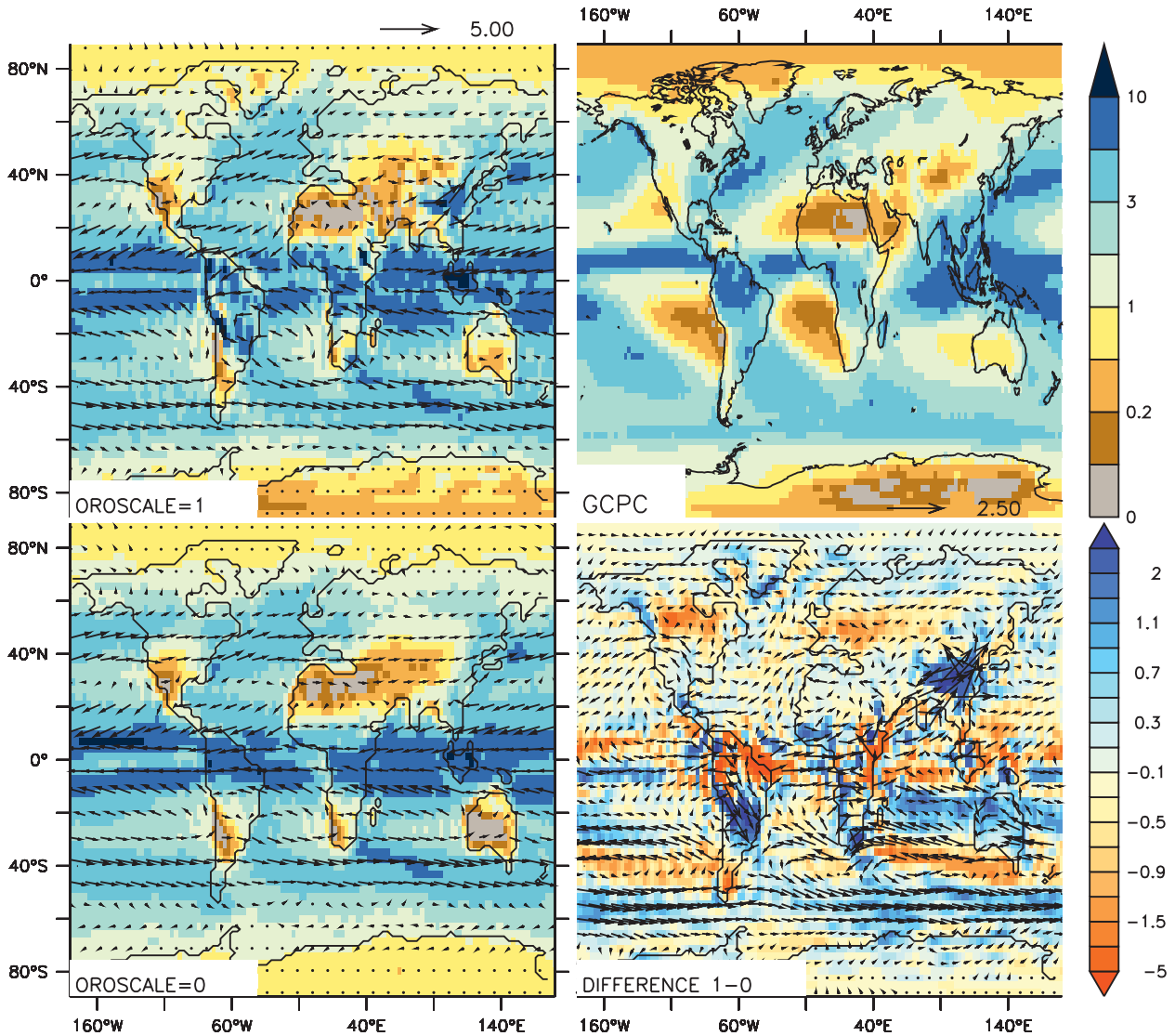


FIG. 9. Latitude-longitude maps of annual mean precipitation ( $\text{mm day}^{-1}$ , color contours) from (top) observations (GPCP, Xie et al. 2003) and vertically integrated moisture transport ( $\int uq\rho dz$ ;  $10^5 \text{ kg m}^{-1} \text{ s}^{-1}$ , arrows) for model (left top) with mountains (OROSCALE = 1) and (left bottom) without mountains (OROSCALE = 0) calculated from daily data from years 20–22. (bottom right) Difference OROSCALE = 1 minus OROSCALE = 0. The left (bottom right) panel(s) show vectors every fourth (third) grid point in longitude and every third (second) grid point in latitude. In the bottom-right panel, the same vector length as in the upper two panels corresponds to half the amount of moisture transport.

contribute to a total of  $\sim 0.13$  Sv of additional surface freshwater input into the Pacific in the models with high orography (OROSCALE = 1.5 and OROSCALE = 1) compared to those with low orography (OROSCALE = 0.5 and OROSCALE = 0). Removing mountains (OROSCALE = 0) leads to more freshwater lost by the Pacific ( $\sim 0.18$  Sv) than by the Atlantic ( $\sim 0.15$  Sv), whereas in the presence of mountains (OROSCALE = 1), the Atlantic loses considerably more freshwater ( $\sim 0.3$  Sv) at the surface than the Pacific ( $\sim 0.05$  Sv).

In the Indian Ocean north of  $35^\circ\text{S}$ , a combination of more river runoff (by up to  $0.1$  Sv), decreased evaporation

(by  $0.1$  Sv), and similar precipitation lead to about  $0.2$  Sv more freshwater input for the high orography (OROSCALE = 1.5) compared with the no orography case (not shown). The effect of present-day mountains is to decrease the amount of freshwater lost at the surface of the Indian Ocean from  $\sim 0.23$  Sv (OROSCALE = 0) to  $\sim 0.13$  Sv (OROSCALE = 1).

### c. Precipitation

The importance of the initial differences in precipitation over the Atlantic Ocean basin between the experiments with (OROSCALE = 1) and without (OROSCALE = 0)

ography in determining the fate of the AMOC, as argued in the previous subsection, warrants more detailed analysis of precipitation and water vapor transport during the early stages of the model integration. The presence of mountains and ice sheets results in decreased precipitation over most of the Atlantic Ocean that dominates the surface freshwater budget between 10° and 60°N (Fig. 8). River runoff decreases at midlatitudes north of 45°N and in the Arctic and shows large changes of both signs in the tropics, decreasing north of the equator and increasing south of the equator. Evaporation shows changes of both signs at midlatitudes and in the tropics. Runoff to the Arctic from all Eurasian and North American rivers is reduced because of the presence of orography because precipitation over North America and Eurasia is decreased (Fig. 9), as described in more detail below. These differences in Arctic river runoff could affect the density of waters flowing over the sills between Greenland and Scotland, which are important components of the NADW and modulate the strength of the AMOC (Döscher and Redler 1997; Schweckendiek and Willebrand 2005).

Low-level winds and resulting moisture transport vectors are much more zonal in the case without mountains (Fig. 9), particularly across North and South America, Europe, and Asia but also over the North Atlantic. The effect of mountains on precipitation therefore exhibits complex spatial patterns determined by both local orographic effects, such as uplift of air masses and wetter conditions upstream and drying in the lee of mountain ranges, and changes in large-scale circulation and humidity convergence–divergence. Generally, our results are similar to earlier studies (Kitoh 2002; Manabe and Terpstra 1974).

Direct orographic effects can be observed over northwest America, where uplift of moist Pacific air masses leads to increased precipitation along the northwestern slopes of the Rocky Mountains. As a result, less water vapor is transported into the interior of the continent, leading to dryer conditions inland. Similar continental drying can be observed over Europe and central Asia. Over Southeast Asia, however, the presence of the Himalayas increases precipitation. The presence of the Andes leads to southward low-level flow over South America with a corresponding shift in precipitation from the equator toward the subtropics. Australia becomes wetter because of the presence of mountains, which lead to decreased divergence of water vapor. The southward shift of the midlatitude westerlies in the Southern Hemisphere is associated with a corresponding southward shift of precipitation.

Precipitation is generally not very well simulated by the model. Although it reproduces some of the large-scale features apparent in the observations—such as low

TABLE 1. Metrics for agreement between models and observations from the GPCP (Huffman et al. 1997) for the spatial distribution of the logarithm of annual mean precipitation  $\log(P)$ : correlation coefficient  $r$  and root-mean-square error (RMSE) normalized by standard deviation of observations.

OROSCALE	0	0.5	1	1.5
$r$	0.60	0.62	0.64	0.62
RMSE	0.92	0.88	0.86	0.89

precipitation over landmasses of North Africa, the Middle East, central Asia, Australia, South Africa, southwestern South America, and Antarctica; and high precipitation in the tropics, over the northwestern midlatitude ocean basins, and the Southern Ocean—regions of low precipitation over the subtropical oceans are not well captured, and rainfall is overestimated there and in the eastern tropical South Pacific and tropical South Atlantic. The latter bias contributes to larger-than-observed precipitation over the Atlantic [ $\sim 2.5$ – $2.9$  Sv, Fig. 7, vs 2.0 Sv in the Global Precipitation Climatology Project (GPCP) observational estimates]. Annual and long-term mean precipitation patterns are in best agreement with observations for the simulation with realistic orography (OROSCALE = 1; Table 1).

#### d. Atmospheric circulation

The zonal-mean circulation in the simulation with mountains is in good agreement with the NCEP reanalysis (Fig. 10). The Hadley cell in boreal summer is  $16 \times 10^{10} \text{ kg s}^{-1}$  and hence just slightly weaker than in the reanalysis ( $18 \times 10^{10} \text{ kg s}^{-1}$ ) and extends not quite far enough north. The austral summer Hadley cell is slightly stronger ( $18 \times 10^{10} \text{ kg s}^{-1}$ ) than in the reanalysis ( $16 \times 10^{10} \text{ kg s}^{-1}$ ). The Northern Hemisphere winter zonal wind jet is slightly narrower and faster ( $50 \text{ m s}^{-1}$ ) than in the reanalysis ( $40 \text{ m s}^{-1}$ ). The Southern Hemisphere winter zonal wind jet is broader than that of the Northern Hemisphere—in agreement with the reanalysis—although the model does not capture the second poleward wind maximum at 100 hPa, presumably because the stratosphere is not resolved. In winter the reanalysis shows a strong polar overturning cell over the Antarctic, whereas no such cell is apparent over the Arctic. The model reproduces this difference between the hemispheres.

Note that the polar winter overturning cell over Antarctica vanishes in the model without mountains and ice sheets, suggesting that this cell is a consequence of the Antarctic ice sheet. We hypothesize that the lack of a lower atmosphere in the presence of the Antarctic ice sheet and the associated reduction of upward longwave radiation leads to less heating and colder temperatures in those mid-lower-tropospheric air layers directly above

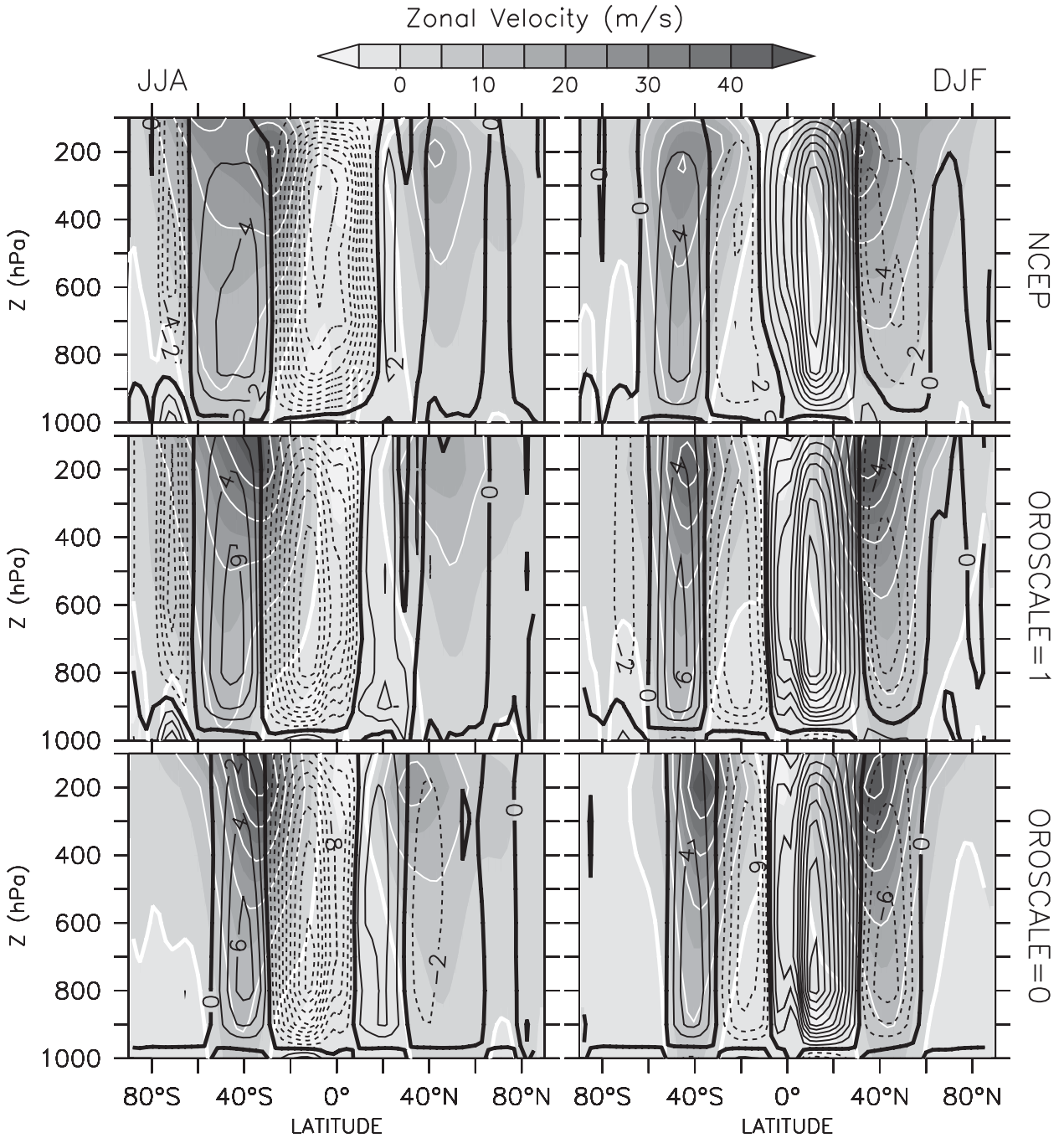


FIG. 10. Atmospheric circulation plotted for (left) austral winter and (right) boreal winter [December–February (DJF)] for (top) the NCEP reanalysis, (middle) the model with realistic mountains (OROSCALE = 1), and (bottom) the model with no mountains (OROSCALE = 0). Model results were averaged between model years 490 and 510. Black lines show the meridional streamfunction ( $10^{10} \text{ kg s}^{-1}$ ), where values (positive, solid; negative, dashed) indicate motion (clockwise; counterclockwise). Gray shading depicts the zonal-mean zonal flow ( $\text{m s}^{-1}$ ) with  $5 \text{ m s}^{-1}$  isotach difference and white lines at  $10 \text{ m s}^{-1}$  isotach difference.

the ice sheet (Fig. 11). Cooler winter air temperatures reduce the geopotential height at 500 hPa ( $Z_{500}$ ) over Antarctica and steepen the pole-to-equator gradient of  $Z_{500}$  from about 650 to about 1000 m. Averaged zonally

and over the year,  $Z_{500}$  is more than 250 m lower over Antarctica than over the Arctic in model OROSCALE = 1 and in the reanalysis, whereas it is identical at both poles in model OROSCALE = 0 (not shown).

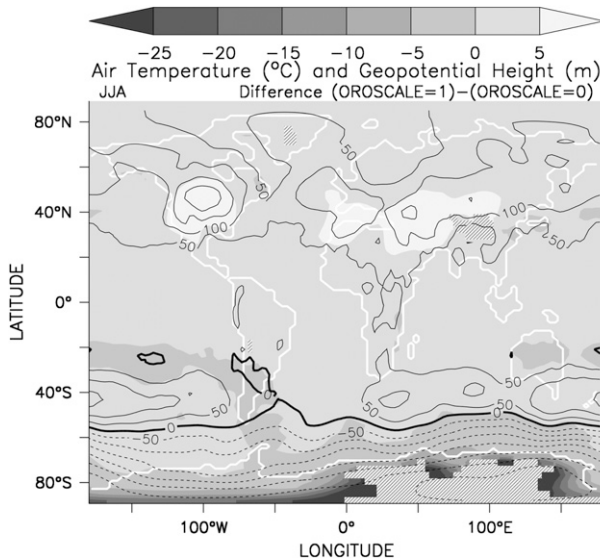


FIG. 11. Horizontal map of differences in air temperature at 750 hPa (grayscale) and geopotential height at 500 hPa (contour lines; negative values are shown as dashed lines) during austral winter between the model with (OROSCALE = 1) and without (OROSCALE = 0) mountains and ice sheets averaged between model years 490 and 510. The diagonally striped pattern corresponds to areas below orography in model OROSCALE = 1. The thick white line indicates the land–sea distribution.

The increased meridional temperature gradients in winter due to the presence of the Antarctic ice sheet sets up a thermally direct overturning circulation with the characteristic katabatic winds—strong boundary layer flow down the ice sheets' slopes (Egger 1985; James 1989; Parish et al. 1993). Moreover, the zonal component of the jet stream in winter is much narrower, faster, and shifted equatorward in the flat-world model consistent with the shift in the surface zonal wind stress maximum (Fig. 5).

#### e. Air temperature

The zonal-mean air temperature in the model with mountains and ice sheets is generally in agreement with the reanalysis (Fig. 12). The isotherms in the presence of the Antarctic ice sheet are vertical in austral winter [June–August (JJA)], consistent with the polar overturning cell leading to descending cold air from the upper troposphere to the surface at high latitudes and strong northward katabatic flow down the slopes of the ice sheet. Because of the absence of this circulation and increased heating from upward longwave radiation, the meridional temperature gradient in the lower troposphere is much smaller in the Arctic.

This difference between the hemispheres is not present in the simulation without mountains and ice sheets. High southern latitudes are much warmer in the lower troposphere in winter; sea ice cover is reduced dramatically

from  $\sim 15.5 \times 10^{-12} \text{ m}^2$ , which is close to the observed value of  $18 \times 10^{-12} \text{ m}^2$  (Cavaliere et al. 2003), to  $3.5 \times 10^{-12} \text{ m}^2$ ; and the meridional temperature gradients are strongly reduced. Smaller meridional temperature gradients lead to a decrease of the high-latitude zonal winds via the thermal wind balance.

This suggests that the presence of the Antarctic ice sheet leads to the observed broader zonal wind jet in the Southern Hemisphere, which is also more extended toward high latitudes, compared with the Northern Hemisphere.

We conclude that the Antarctic ice sheet draws the surface westerlies southward by increasing the meridional temperature gradient in the lower troposphere.

#### f. Eddy kinetic energy

A quantitative theory predicting surface westerly winds at midlatitudes remains lacking. Nevertheless, baroclinic eddies remove zonal momentum from the mean flow in the upper troposphere and transport it toward the surface (Gill 1982). This is part of the large-scale meridional transport of angular momentum from the low-latitude surface of the earth via the atmosphere to the higher-latitude surface (Hartmann 1994). In light of the important role of transient eddies in the zonal momentum transport it, will be useful to analyze the changes in eddy kinetic energy.

Figure 13 shows that the removal of mountains and ice sheets reduces the stationary eddy kinetic energy and increases the transient eddy kinetic energy, consistent with Manabe and Terpstra (1974). The largest increase in vertically averaged transient eddy kinetic energy occurs in winter in the Northern Hemisphere, where the maximum around  $40^\circ\text{N}$  increases by more than 50% from less than  $80 \text{ m}^2 \text{ s}^{-2}$  to more than  $120 \text{ m}^2 \text{ s}^{-2}$ . Note that the latitude of the maximum eddy activity does not shift. A more efficient transfer of zonal momentum from the upper troposphere to the surface by increased transient eddy activity is consistent with the increase in surface westerly winds in the Northern Hemisphere in the simulation without mountains (Fig. 5).

In the Southern Hemisphere, the maximum of transient eddy kinetic energy has not increased; however, it is shifted northward by about  $10^\circ$ , and the peak is sharper in the simulation without mountains, consistent with the shift in surface westerlies (Fig. 5) and meridional water vapor transport (Fig. 9).

## 6. Discussion and implications

We have argued that the presence of the Antarctic ice sheet leads to a fundamentally different atmospheric meridional overturning circulation in winter in the Southern Hemisphere compared with the Northern Hemisphere, which increases the meridional temperature gradient and

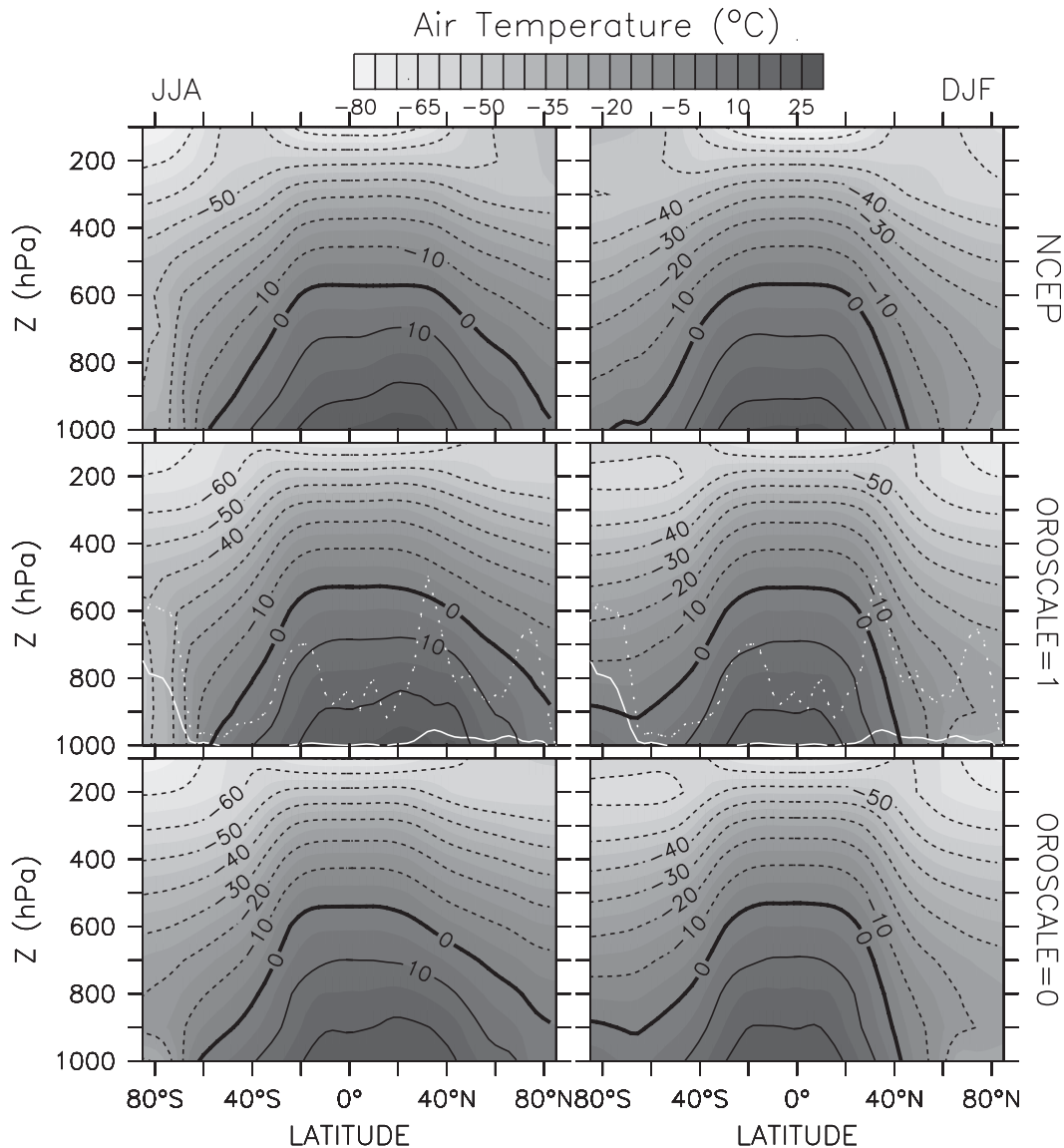


FIG. 12. Zonal-mean air temperature during (left) austral winter and (right) boreal winter for (top) the NCEP reanalysis, (middle) the model with realistic mountains (OROSCALE = 1), and (bottom) the model with no mountains (OROSCALE = 0). Model results were averaged between model years 490 and 510. Solid (dotted) white lines in (top) show zonal mean (maximum) orography.

draws the westerly winds southward. This argument was supported by the difference between the hemispheres in the observations, as approximated by the NCEP–National Center for Atmospheric Research (NCAR) reanalysis (Figs. 9 and 10). The reanalysis, which covers 40 yr from 1957 to 1997, probably includes anthropogenic trends. Stratospheric ozone depletion has increased the Antarctic polar vortex and westerly winds during the past 30 yr (Gillett and Thompson 2003; Thompson and Solomon 2002). However, the anthropogenic changes occurred in austral summer and do not affect our conclusions much, which are based on winter data.

In contrast to the large sensitivity of surface zonal winds to the presence of mountains that we find in OSUVic, Kitoh (2002) did not seem to find an appreciable response in the Meteorological Research Institute (MRI) coupled atmosphere–ocean general circulation model, perhaps because of the coarse horizontal resolution of  $4^\circ \times 5^\circ$ , which corresponds to about T21. A more recent study by Kitoh (2004) at T42 resolution does not explicitly show surface wind stress, making a quantitative comparison difficult. OSUVic is simplified in many ways. In particular, the coarse vertical resolution with only 10 layers may be leading to some systematic model biases and may explain

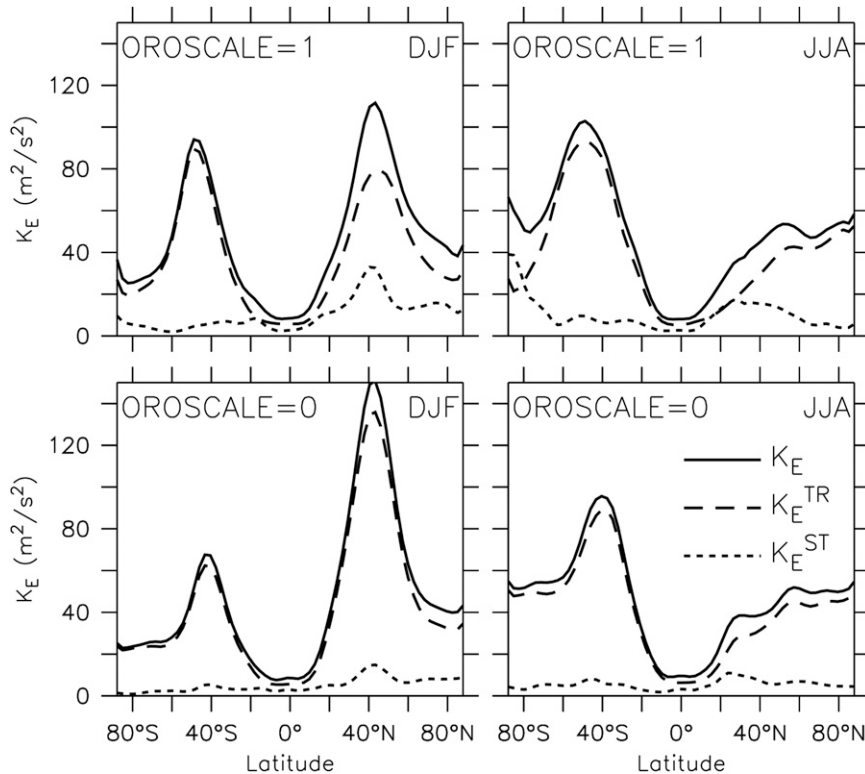


FIG. 13. Zonal- and vertical-mean eddy kinetic energy for (top) the model with mountains and (bottom) the model without mountains for (left) Northern Hemisphere winter (DJF) and (right) Southern Hemisphere winter (JJA). Solid lines show total eddy kinetic energy  $K_E = K_E^{TR} + K_E^{ST}$ , dashed lines show transient eddy kinetic energy  $K_E^{TR} = 0.5[\overline{u'^2} + \overline{v'^2}]$ , and dotted lines show the stationary eddy kinetic energy  $K_E^{ST} = 0.5[\overline{u'^*2} + \overline{v'^*2}]$ , where overbars denote time averages, square brackets indicate zonal averages, and primes and asterisks indicate deviations from the time and zonal averages, respectively (Peixoto and Oort 1992). Daily data from 5 yr of model output at the end of the simulation have been used to calculate the average kinetic energy over that period.

possible differences with Kitoh (2004). Also note that OSUVic does not use a parameterization of gravity-wave drag, which is known to slow down surface westerlies (Boer and Lazare 1988). Repeating simulations with different orography using a state-of-the-art climate model would therefore be desirable, particularly with respect to the surface wind response.

Our results may have implications for paleoclimates and/or future scenarios, particularly periods without the Antarctic ice sheet, suggesting that Southern Hemisphere winds were shifted northward and weaker before the glacial inception of Antarctica, with possibly important consequences for the carbon cycle.

## 7. Conclusions

Our numerical experiments show a strong influence of mountains and ice sheets on the general circulation of the ocean. Deep-water formation and meridional overturning circulation is stronger in the Atlantic and weaker in the

Pacific the higher the orography. In a model world without mountains and ice sheets, deep water forms in the North Pacific and not in the North Atlantic—contrary to modern observations. The ACC is stronger and upwelling

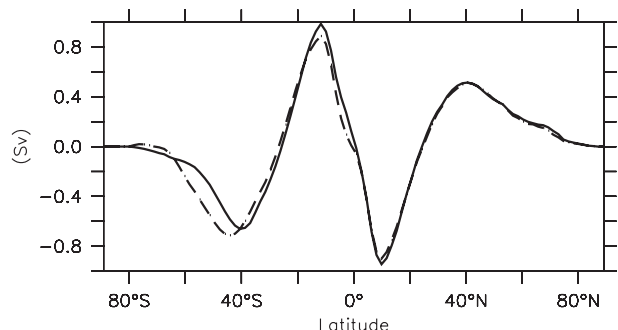


FIG. 14. Northward meridional water vapor transport in the atmosphere from the model without mountains (OROSCALE = 0; solid line) and the model with mountains (OROSCALE = 1; dashed line).

is shifted 10° southward because of the presence of the Antarctic ice sheet. We have identified two main mechanisms explaining the strong influence of orography on the ocean circulation.

First, the Atlantic becomes saltier the higher the mountains are, and the Pacific becomes fresher. This is explained by the presence of the Andes and the Rocky Mountains, which block atmospheric water vapor transport from the Pacific to the Atlantic at midlatitudes, whereas the trade winds move water vapor across the Central American isthmus from the Atlantic to the Pacific. Increased salinities in the North Atlantic promote deep-water formation and accelerate the AMOC, whereas the North Pacific becomes more stratified.

Second, zonal wind stress over the Southern Ocean is increased and shifted southward by the presence of the Antarctic ice sheet. This increases the ACC and shifts the upwelling of deep water in the Southern Ocean poleward and intensifies it. Stronger zonal wind stress over the Southern Ocean has been shown to increase the sinking rate of the NADW and the AMOC (Toggweiler and Samuels 1995), although presumably not as much as initially suggested (Delworth and Zeng 2008; Rahmstorf and England 1997). A southward shift of the westerlies intensifies the surface return flow of salty Indian Ocean water along the “warm-water route” around the southern tip of Africa into the Atlantic (Agulhas leakage; Fig. 4). (The “cold-water route” from the Pacific around the tip of South America occurs at higher latitudes and is therefore fresher.) Increased Agulhas leakage has been shown to increase the salinity of the Atlantic and the AMOC (Sijp and England 2009). A southward shift of the westerly winds leads to a southward shift of the storm tracks and increased atmospheric meridional moisture transport by transient eddies (Figs. 9 and 14), which has been shown to increase the AMOC by freshening Southern Hemisphere deep water (Saenko et al. 2003b).

These two processes—less atmospheric water vapor export from the Pacific to the Atlantic drainage basin and southward-shifted Southern Hemisphere westerlies—thus combine to enhance deep-water formation in the North Atlantic and accelerate the Atlantic meridional overturning circulation in the presence of mountains and ice sheets. Future studies and additional sensitivity experiments will be required to quantify the relative roles of these two mechanisms. We conclude that the present configuration of mountains and ice sheets on Earth is key to determining the observed global circulation pattern of the contemporary ocean.

*Acknowledgments.* This work was supported as part of project PALEOVAR by the NSF paleoclimate program Grant ATM-0602395 to AS. KF, FL, and EK received

funding through the DFG Project FR 450/10-1. KF, Max Planck Fellow, acknowledges support by the Max Planck Society. Constructive comments from three anonymous reviewers and from Marika Holland (editor) were appreciated and helped to improve the manuscript.

## APPENDIX

### Effects of Atmospheric Model Resolution on Ocean Circulation

#### *a. Discussion*

The reasons for the weaker AMOC in the T21 model version compared with the T42 model version are not entirely clear. The Atlantic surface freshwater budget is more evaporative for the T21 model (Fig. 6) and hence cannot be part of the explanation. Redistribution of freshwater within the Atlantic drainage basin diagnosed from (not shown) decreased precipitation and runoff in the tropics, and reduced evaporation and increased river runoff north of 25°N contributes to higher salinities at low latitudes and lower salinities at high latitudes in the T21 model version. In addition, the much weaker and northward-shifted zonal wind stress in the Southern Hemisphere (Fig. 5) will undoubtedly contribute to the weaker AMOC in the T21 model for reasons similar to those discussed in the main text.

Our results are consistent and provide an explanation for the diagnosis of Bryan et al. (2006), that in the National Center for Atmospheric Research (NCAR) Community Climate System Model, version 3 (CCSM3), the AMOC increases with increasing atmospheric model resolution. Our results are also consistent with a too low AMOC and too weak and northward-displaced maximum surface wind stress maximum in the Southern Hemisphere in the T31-resolution model GENMOM (derived from combining the Global Environmental and Ecological Simulation of Interactive Systems, or GENESIS, and Modular Ocean Model GCMs; Alder et al. 2010). This raises the question at what resolution convergence of the simulated AMOC with respect to horizontal model resolution can be expected. The results by Bryan et al. (2006), who show a large increase in the AMOC between T31 and T42 from 15.3 to 19.5 Sv and a smaller increase to 21.8 Sv at T85 resolution, suggest that convergence of the AMOC occurs somewhere between T42 and T85, perhaps closer to T42, although even higher-resolution runs would be necessary to prove that assertion. Our OSUVic results support that rough estimate.

Differences in surface zonal wind stress between the T21- and T42-resolution versions (Fig. 5) are most likely dominated by meridional resolution as demonstrated

earlier (Held and Phillipps 1993; Tibaldi et al. 1990) and not by the representation of orography. Our OSUVic results are consistent with earlier work (Tibaldi et al. 1990) that indicates that convergence of the Southern Hemisphere wind stress appears to occur around T42 resolution.

### b. Implications

Our results have implications for results from climate models at low resolution, which are frequently used for paleoclimate applications because of the long time integrations necessary. Many of these models use flux corrections to simulate a reasonable AMOC. Goosse et al. (2002), for example, require to remove freshwater from the Atlantic in the widely used ECBILT-CLIO model [more recently also known as Loch-Vecode-ECBILT-CLIO-AGISM Model (LOVECLIM)] at T21 resolution to simulate a reasonable AMOC, yet this model has been used frequently to study AMOC variability and feedbacks (e.g., Krebs and Timmermann 2007; Okazaki et al. 2010). This is also true for the widely used Grid Enabled Integrated Earth system, version 2 (GENIE-2) model at T21 resolution (Lenton et al. 2007). OSUVic at T21 resolution also simulates a much too weak AMOC (~9 Sv). The requirement for flux corrections suggests that the model does not correctly capture one or more important processes. Two important processes that strongly influence the simulation of the AMOC are the Atlantic surface freshwater budget and the wind stress over the Southern Ocean. Here we have shown that both depend strongly on orography, the representation of which at low resolution (e.g., T21, see Fig. 1) is insufficient (Fig. 5). The results from the applications of these models to climates different from today therefore have to be regarded with reservation.

The importance of Southern Hemisphere westerly winds for ocean circulation and biogeochemical cycling are well known (Sarmiento et al. 2004). Problems of low-resolution models in simulating Southern Hemisphere winds may explain the inconsistencies of the carbon cycle response between some of these models (Menviel et al. 2008; Schmittner and Galbraith 2008). Moreover, the simulation of the Southern Ocean circulation remains challenging for coupled climate models (Russell et al. 2006), perhaps in some cases because of too low resolution.

The original purpose of the UVic-Planet Simulator model coupling exercise was to create a computationally efficient climate model for paleoclimate applications. However, the major biases (e.g., in surface wind stress and AMOC) we found in the T21 model version imply that this model version cannot be used for realistic paleoclimate applications. We argue that using a model with known large biases, even if some of those biases can be eliminated with flux corrections, leaves the results highly

unreliable. Some of the issues of low-resolution models may be fixed in the future by clever subgrid-scale parameterizations. For example, it is conceivable to develop a subgrid-scale scheme of precipitation calculations, considering a high-resolution orography. Until then, however, low-resolution model results have to be regarded with skepticism.

### REFERENCES

- Alder, J. R., S. W. Hostetler, D. Pollard, and A. Schmittner, 2010: Evaluation of a present-day climate simulation with a new coupled atmosphere-ocean model GENMOM. *Geosci. Model Dev. Discuss.*, 1697–1735.
- Antonov, J. I., R. A. Locarni, T. P. Boyer, A. V. Mishonov, and H. E. Garcia, 2006: *Salinity*. Vol. 2, *World Ocean Atlas 2005*, NOAA Atlas NESDIS 62, 182 pp.
- Boer, G. J., and M. Lazare, 1988: Some results concerning the effect of horizontal resolution and gravity-wave drag on simulated climate. *J. Climate*, **1**, 789–806.
- Broecker, W. S., D. R. Peteet, and D. Rind, 1985: Does the ocean-atmosphere system have more than one stable model of operation? *Nature*, **315**, 21–26.
- Bryan, F. O., G. Danabasoglu, N. Nakashiki, Y. Yoshida, D. H. Kim, J. Tsutsui, and S. C. Doney, 2006: Response of the North Atlantic thermohaline circulation and ventilation to increasing carbon dioxide in CCSM3. *J. Climate*, **19**, 2382–2397.
- Cavaliere, D. J., C. L. Parkinson, and K. Y. Vinnikov, 2003: 30-year satellite record reveals contrasting Arctic and Antarctic decadal sea ice variability. *Geophys. Res. Lett.*, **30**, 1970, doi:10.1029/2003GL018031.
- Delworth, T. L., and F. R. Zeng, 2008: Simulated impact of altered Southern Hemisphere winds on the Atlantic meridional overturning circulation. *Geophys. Res. Lett.*, **35**, L20708, doi:10.1029/2008GL035166.
- Dietrich, G., and K. Kalle, 1957: *Allgemeine Meereskunde: Eine Einführung in die Ozeanographie*. Gebrüder Borntraeger, 492 pp.
- Döscher, R., and R. Redler, 1997: The relative importance of northern overflow and subpolar deep convection for the North Atlantic thermohaline circulation. *J. Phys. Oceanogr.*, **27**, 1894–1902.
- Egger, J., 1985: Slope winds and the axisymmetric circulation over Antarctica. *J. Atmos. Sci.*, **42**, 1859–1867.
- Fraedrich, K., H. Jansen, E. Kirk, U. Luksch, and F. Lunkeit, 2005a: The Planet Simulator: Towards a user friendly model. *Meteor. Z.*, **14**, 299–304.
- , —, —, and F. Lunkeit, 2005b: The Planet Simulator: Green planet and desert world. *Meteor. Z.*, **14**, 305–314.
- Gill, A. E., 1982: *Atmosphere-Ocean Dynamics*. Academic Press, 662 pp.
- Gillett, N. P., and D. W. J. Thompson, 2003: Simulation of recent Southern Hemisphere climate change. *Science*, **302**, 273–275.
- Goosse, H., F. M. Selten, R. J. Haarsma, and J. D. Opsteegh, 2002: A mechanism of decadal variability of the sea-ice volume in the Northern Hemisphere. *Climate Dyn.*, **19**, 61–83.
- Gregory, J. M., O. A. Saenko, and A. J. Weaver, 2003: The role of the Atlantic freshwater balance in the hysteresis of the meridional overturning circulation. *Climate Dyn.*, **21**, 707–717.
- Hartmann, D. L., 1994: *Global Physical Climatology*. Academic Press, 411 pp.
- Held, I. M., and P. J. Phillipps, 1993: Sensitivity of the eddy momentum flux to meridional resolution in atmospheric GCMs. *J. Climate*, **6**, 499–507.

- Huffman, G. J., and Coauthors, 1997: The Global Precipitation Climatology Project (GPCP) combined precipitation dataset. *Bull. Amer. Meteor. Soc.*, **78**, 5–20.
- James, I. N., 1989: The Antarctic drainage flow: Implications for hemispheric flow on the Southern Hemisphere. *Antarct. Sci.*, **1**, 279–290.
- Kalnay, E., and Coauthors, 1996: The NCEP/NCAR 40-Year Reanalysis Project. *Bull. Amer. Meteor. Soc.*, **77**, 437–471.
- Kitoh, A., 2002: Effects of large-scale mountains on surface climate—A coupled ocean-atmosphere general circulation model study. *J. Meteor. Soc. Japan.*, **80**, 1165–1181.
- , 2004: Effects of mountain uplift on East Asian summer climate investigated by a coupled atmosphere–ocean GCM. *J. Climate*, **17**, 783–802.
- Krebs, U., and A. Timmermann, 2007: Tropical air–sea interactions accelerate the recovery of the Atlantic meridional overturning circulation after a major shutdown. *J. Climate*, **20**, 4940–4956.
- Lenton, T. M., and Coauthors, 2007: Effects of atmospheric dynamics and ocean resolution on bi-stability of the thermohaline circulation examined using the Grid Enabled Integrated Earth system modelling (GENIE) framework. *Climate Dyn.*, **29**, 591–613.
- Locarni, R. A., A. V. Mishonov, J. I. Antonov, T. P. Boyer, and H. E. Garcia, 2006: *Temperature*. Vol. 1, *World Ocean Atlas 2005*, NOAA Atlas NESDIS 61, 182 pp.
- Lohmann, G., 2003: Atmospheric and oceanic freshwater transport during weak Atlantic overturning circulation. *Tellus*, **55**, 438–449.
- Lumpkin, R., and K. Speer, 2007: Global ocean meridional overturning. *J. Phys. Oceanogr.*, **37**, 2550–2562.
- Manabe, S., and T. B. Terpstra, 1974: The effects of mountains on the general circulation of the atmosphere as identified by numerical experiments. *J. Atmos. Sci.*, **31**, 3–42.
- , and R. J. Stouffer, 1994: Multiple-century response of a coupled ocean–atmosphere model to an increase of atmospheric carbon dioxide. *J. Climate*, **7**, 5–23.
- Marshall, J., and T. Radko, 2003: Residual-mean solutions for the Antarctic Circumpolar Current and its associated overturning circulation. *J. Phys. Oceanogr.*, **33**, 2341–2354.
- McDermott, D. A., 1996: The regulation of northern overturning by Southern Hemisphere winds. *J. Phys. Oceanogr.*, **26**, 1234–1255.
- Menziel, L., A. Timmermann, A. Mouchet, and O. Timm, 2008: Meridional reorganizations of marine and terrestrial productivity during Heinrich events. *Paleoceanography*, **23**, PA1203, doi:10.1029/2007PA001445.
- Okazaki, Y., A. Timmermann, L. Menziel, N. Harada, A. Abe-Ouchi, M. O. Chikamoto, A. Mouchet, and H. Asahi, 2010: Deepwater formation in the North Pacific during the last glacial termination. *Science*, **329**, 200–204.
- Parish, T. R., P. Pettré, and G. Wendler, 1993: The influence of large-scale forcing on the katabatic wind regime at Adélie Land, Antarctica. *Meteor. Atmos. Phys.*, **51**, 165–176.
- Peixoto, J. P., and A. H. Oort, 1992: *Physics of Climate*. Springer, 520 pp.
- Rahmstorf, S., 1996: On the freshwater forcing and transport of the Atlantic thermohaline circulation. *Climate Dyn.*, **12**, 799–811.
- , and M. H. England, 1997: Influence of Southern Hemisphere winds on North Atlantic deep water flow. *J. Phys. Oceanogr.*, **27**, 2040–2054.
- Russell, J. L., R. J. Stouffer, and K. W. Dixon, 2006: Intercomparison of the Southern Ocean circulations in IPCC coupled model control simulations. *J. Climate*, **19**, 4560–4575.
- Saenko, O. A., A. J. Weaver, and J. M. Gregory, 2003a: On the link between the two modes of the ocean thermohaline circulation and the formation of global-scale water masses. *J. Climate*, **16**, 2797–2801.
- , —, and A. Schmittner, 2003b: Atlantic deep circulation controlled by freshening in the Southern Ocean. *Geophys. Res. Lett.*, **30**, 1754, doi:10.1029/2003GL017681.
- Sarmiento, J. L., N. Gruber, M. A. Brzezinski, and J. P. Dunne, 2004: High-latitude controls of thermocline nutrients and low latitude biological productivity. *Nature*, **427**, 56–60.
- Schmittner, A., and E. D. Galbraith, 2008: Glacial greenhouse-gas fluctuations controlled by ocean circulation changes. *Nature*, **456**, 373–376.
- , M. Latif, and B. Schneider, 2005: Model projections of the North Atlantic thermohaline circulation for the 21st century assessed by observations. *Geophys. Res. Lett.*, **32**, L23710, doi:10.1029/2005GL024368.
- , A. Oschlies, H. D. Matthews, and E. D. Galbraith, 2008: Future changes in climate, ocean circulation, ecosystems, and biogeochemical cycling simulated for a business-as-usual CO<sub>2</sub> emission scenario until year 4000 AD. *Global Biogeochem. Cycles*, GB1013, doi:10.1029/2007GB002953.
- Schweckendiek, U., and J. Willebrand, 2005: Mechanisms affecting the overturning response in global warming simulations. *J. Climate*, **18**, 4925–4936.
- Sijp, W. P., and M. H. England, 2009: Southern Hemisphere westerly wind control over the ocean’s thermohaline circulation. *J. Climate*, **22**, 1277–1286.
- Stocker, T. F., and D. G. Wright, 1991: Rapid transitions of the ocean’s deep circulation induced by changes in surface water fluxes. *Nature*, **351**, 729–732.
- Talley, L. D., 2008: Freshwater transport estimates and the global overturning circulation: Shallow, deep and throughflow components. *Prog. Oceanogr.*, **78**, 257–303.
- Thompson, D. W. J., and S. Solomon, 2002: Interpretation of recent Southern Hemisphere climate change. *Science*, **296**, 895–899.
- Tibaldi, S., T. N. Palmer, Č. Branković, and U. Cubasch, 1990: Extended-range predictions with ECMWF models: Influence of horizontal resolution on systematic error and forecast skill. *Quart. J. Roy. Meteor. Soc.*, **116**, 835–866.
- Toggweiler, J. R., and B. Samuels, 1995: Effect of Drake Passage on the global thermohaline circulation. *Deep-Sea Res. I*, **42**, 477–500.
- Warren, B. A., 1983: Why is no deep-water formed in the North Pacific? *J. Mar. Res.*, **41**, 327–347.
- Weaver, A. J., C. M. Bitz, A. F. Fanning, and M. M. Holland, 1999: Thermohaline circulation: High-latitude phenomena and the difference between the Pacific and Atlantic. *Annu. Rev. Earth Planet. Sci.*, **27**, 231–285.
- , and Coauthors, 2001: The UVic Earth System Climate Model: Model description, climatology, and applications to past, present and future climates. *Atmos.–Ocean*, **39**, 361–428.
- Weyl, P., 1968: The role of the oceans in climate change: A theory of the ice ages. *Causes of Climatic Change, Meteor. Monogr.*, No. 30, Amer. Meteor. Soc., 37–62.
- Wunsch, C., and P. Heimbach, 2006: Estimated decadal changes in the North Atlantic meridional overturning circulation and heat flux 1993–2004. *J. Phys. Oceanogr.*, **36**, 2012–2024.
- Xie, P. P., J. E. Janowiak, P. A. Arkin, R. Adler, A. Gruber, R. Ferraro, G. J. Huffman, and S. Curtis, 2003: GPCP pentad precipitation analyses: An experimental dataset based on gauge observations and satellite estimates. *J. Climate*, **16**, 2197–2214.
- Zaucker, F., and W. S. Broecker, 1992: The influence of atmospheric moisture transport on the fresh water balance of the Atlantic drainage basin: General circulation model simulations and observations. *J. Geophys. Res.*, **97**, 2765–2773.